Sketch of LIGO Detectors: Notes

Rhiannon Udall

February 6, 2023

Contents

1 Introduction

Second generation ground based gravitational wave interferometers - LIGO, Virgo, and KAGRA - represent one of the most significant achievements in human history. They are the most sensitive scientific observing instruments ever constructed, and represent the culmination of decades of work. As one might expect, they are also fiendishly complex, to the point that fully understanding even one part of their construction and operation is the content of a PhD. The aim of this talk is to provide an introduction to the LIGO detectors, one step past that which is usually presented. There will be massive omissions in this talk, including both controls systems and mode cleaning, which are absolutely critical elements of the detector. However, attention will be given to the use of cavities to enhance the detector, the actual behavior of the detection scheme, and some of the fundamental noise sources in the detector. In what is covered, this follows Bond et al [1], but that review article is *much* more extensive, and is worth a look for the interested. All figures are also taken from that review article, and all intellectual credit should be paid due to its authors.

1.1 Gravitational Waves in Brief

Gravitational waves are distortions in spacetime, generated whenever there is a change in mass moments of quadrupolar order or higher. For a quadrupolar (the dominant radiation mode), the strain may be written [2]

$$h_{ij} = \frac{2}{c^4}\frac{G}{D_L}\frac{d^2Q_{ij}}{dt^2} \tag{1}$$

Where G and c are the standard constants, D_L is the luminosity distance, and Q_{ij} is the mass quadrupolar moment of the system. Two pieces are important here: first, the magnitude is principally is G/c^4 - very small! The second is that the scaling with distance is only inverse, instead of an inverse square. Thus, even though the strain is intrinsically small, it scales much better with distance than electromagnetic sources do. In order to compensate for this, the second derivative in time of the quadrupolar moment must be exceptionally large. There are many ways this can be sourced, but so far (due partially to astrophysics and partly to the nature of the detectors) we have only seen GWs from compact binary coalescences - that is the merger of a black hole or neutron star with another black hole or neutron star.

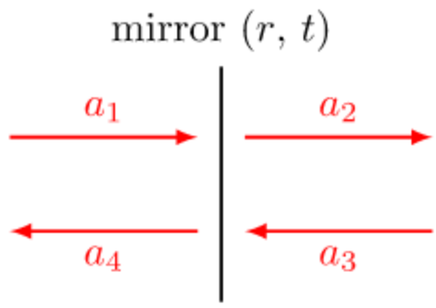

Figure 1: An illustration of the idealized mirror

The next question one may ask is: what is this strain of which you speak? Strain as written above is a tensorial quantity. Through some math this talk will not be going into, this may be written in two components: h_+ and $h_\times$, which are typically of similar magnitudes The important bit here is that the detectors we will be discussing have a characteristic response, called the antenna response. For Michelson interferometers like ours, this combines as:

$$h = \frac{L_X - L_Y}{L} = F_+ h_+ + F_\times h_\times \tag{2}$$

Where L_X, L_Y are the lengths of respective arms, and L is the typical detector length. So, our goal is to measure extremely small - $O(10^{-21})$ - differences in the lengths of the detector arms.

2 Building Blocks: Cavities and Michelson Interferometers

2.1 Fabry-Perot Cavities

Let's recall some electromagnetism. We can characterize light by it's electric field, which - if we ignore polarization and assume propagation along the z-axis - can give

$$E = \mathcal{R}(E_0' \exp(i(\omega t - kz)) \tag{3}$$

Where E_0' is a complex number that folds in the initial phase. For this we will be interested in the instantaneous field at $t = 0$, and will focus on the complex amplitudes, so

$$E = E_0 \exp(-ikz) \tag{4}$$

2.1.1 Interaction with Mirrors

Now, how will this interact with mirrors, or propagate through space? For mirrors we have the setup in Figure 1. We can write out a system of equations for this:

$$a_2 = ita_1 + ra_3 \tag{5}$$

$$a_4 = ita_3 + ra_1 \tag{6}$$

Here we assume that transmission applies a phase shift of $\pi/2$. [1] has an elaborate explanation of why this assumption will generally hold, but for our purposes we're just going to accept it. We will similarly assume that these are lossless mirrors, so that $r^2 + t^2 = 1$.

For reasons which will become apparent in a moment, let's also rearrange these equations a bit:

$$a_1 = \frac{i}{t}(ra_3 - a_2) \tag{7}$$

$$a_4 = \frac{ri}{t}(ra_3 - a_2) + ita_3 = \frac{i}{t}(a_3 - ra_2) \tag{8}$$

We can reframe this as a matrix equation:

$$\begin{pmatrix} a_1 \\ a_4 \end{pmatrix} = \frac{i}{t}\begin{pmatrix} -1 & r \\ -r & 1 \end{pmatrix}\begin{pmatrix} a_2 \\ a_3 \end{pmatrix} \tag{9}$$

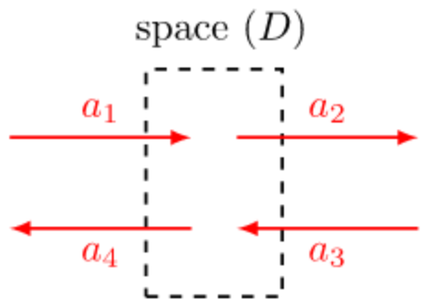

Figure 2: An illustration of scalar wave propagation through space

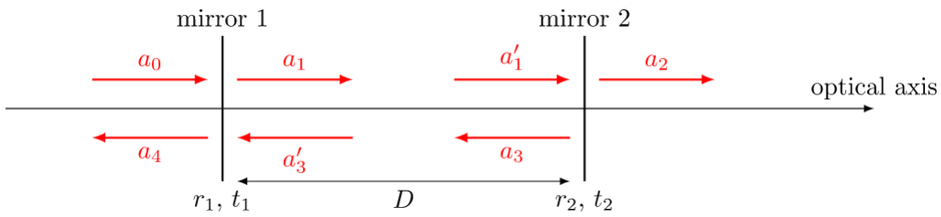

Figure 3: An illustration of the idealized two mirror system

2.1.2 Propagation Through Space

Now for propagation through space, we have the illustration in Figure 2. This gives the system of equations:

$$a_2 = a_1 \exp(-ikD) \tag{10}$$

$$a_4 = a_3 \exp(-ikD) \tag{11}$$

Rearranging a bit is trivial, to get the matrix form for this system:

$$\begin{pmatrix} a_1 \\ a_4 \end{pmatrix} = \begin{pmatrix} \exp(ikD) & 0 \\ 0 & \exp(-ikD) \end{pmatrix} \begin{pmatrix} a_2 \\ a_3 \end{pmatrix} \tag{12}$$

2.1.3 Two Mirror Systems

Now, let's consider a two mirror system, seen in Figure 3. Here the second mirror has no field incoming from the right side, so $a_3 = 0$. The beauty of matrix optics is now revealed: to solve the entire system we simply have

$$\begin{pmatrix} a_0 \\ a_4 \end{pmatrix} = \frac{i}{t_1} \begin{pmatrix} -1 & r_1 \\ -r_1 & 1 \end{pmatrix} \begin{pmatrix} \exp(ikD) & 0 \\ 0 & \exp(-ikD) \end{pmatrix} \frac{i}{t_2} \begin{pmatrix} -1 & r_2 \\ -r_2 & 1 \end{pmatrix} \begin{pmatrix} a_2 \\ 0 \end{pmatrix} \tag{13}$$

Which reduces to

$$\begin{pmatrix} a_0 \\ a_4 \end{pmatrix} = \frac{-1}{t_1 t_2} \begin{pmatrix} \exp(ikD) - r_1 r_2 \exp(-ikD) & -r_2 \exp(ikD) + r_1 \exp(-ikD) \\ -r_2 \exp(ikD) + r_1 \exp(-ikD) & \exp(-ikD) - r_1 r_2 \exp(ikD) \end{pmatrix} \begin{pmatrix} a_2 \\ 0 \end{pmatrix} \tag{14}$$

Which lets us get the expression ratio of the transmitted amplitude to the incoming amplitude:

$$\frac{a_2}{a_0} = \frac{-t_1 t_2 \exp(-ikD)}{1 - r_1 r_2 \exp(-i2kD)} \tag{15}$$

At this point, you are probably saying to yourself "well that's all well and good, but you know, why exactly?" The two mirror system is a Fabry-Pérot interferometer, which has some very important properties. Setting the distance D be the length of the arm L, we can see that if $kL = N\pi$ for $N \in \mathrm{Z}$, then we have a resonance. If instead kL is a half integer multiple of π, then we get an anti-resonance instead. The frequency offset between peaks is called the *free spectral range*, or FSR, and may be found by

$$\mathrm{FSR} = \frac{c}{2L} \tag{16}$$

We can similarly find the line width, or *frequency width at half maximum* (FWHM), which is

$$\mathrm{FWHM} = \frac{2FSR}{\pi} \arcsin\left(\frac{1 - r_1 r_2}{2\sqrt{r_1 r_2}}\right) \tag{17}$$

Together, these also define the finesse of the cavity:

$$F = \frac{\mathrm{FSR}}{\mathrm{FWHM}} = \frac{\pi}{2 \arcsin\left(\frac{1 - r_1 r_2}{2\sqrt{r_1 r_2}}\right)} \tag{18}$$

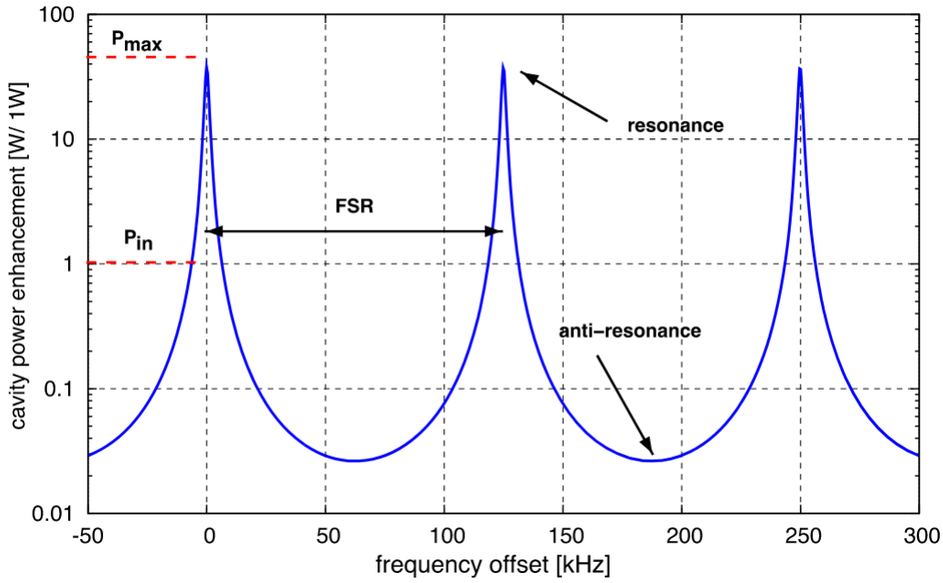

Figure 4: The frequency dependent power enhancement of an example Fabry-Pérot interferometer

Which for r_1, r_2 near 1 (a high finesse cavity) approximates to:

$$F \approx \frac{\pi}{1 - r_1 r_2} \tag{19}$$

As one may note, when a Fabry-Pérot cavity is on resonance, the transmitted power is *much* higher than the input power (see Figure 4. Thus we can essentially "step up" the laser power by this method, at the cost of having added degrees of freedom in our setup which must be controlled. Furthermore, photons in a cavity may traverse the length many times before they are eventually transmitted. For gravitational waves, where maximizing L for fixed strain magnitude h lets us observe ΔL of greater magnitude, this is very advantageous.

2.2 Michelson Interferometers

2.2.1 Output Field due to Phase Shifts

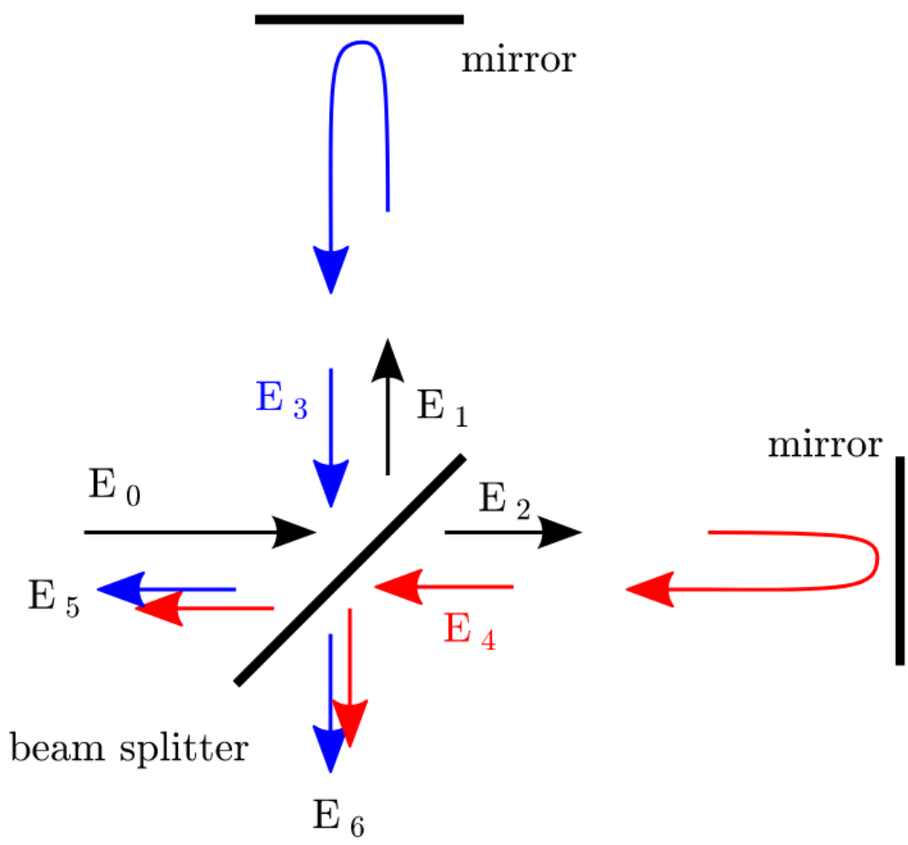

Figure 5: A schematics of optical fields in a simple Michelson interferometer

Now we can talk about Michelson interferometers, the other essential type of optical configuration in the

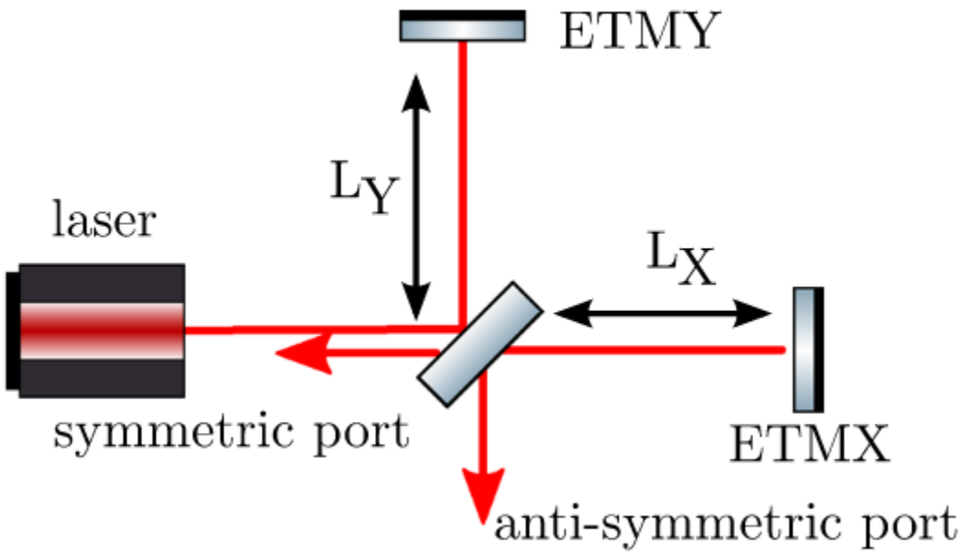

Figure 6: A schematic of the prototypical Michelson interferometer

LIGO interferometers. Figure 5 is a schematic of the fields in a simple Michelson interferometer. We'll skip the rigmarole of getting the field elements, to write out the one most relevant to us:

$$E_6 = E_0 rt\left[\exp\Big(i(\phi_t + \phi_{r1} + \Phi_1)\Big) + \exp\Big(i(\phi_t + \phi_{r2} + \Phi_2)\Big)\right] \tag{20}$$

By some arguments we also won't go into, we can choose a convention of $\phi_t = \pi/2$, $\phi_{r1} = \phi_{r2} = 0$ (this is the same as convention of introducing a factor of i during transmission which was used above). Meanwhile, Φ_1 and Φ_2 are the phase difference picked up along the Y and X arms respectively. So, you can simplify this and combine the common and differential elements:

$$E_6 = irtE_0 \exp\left(i\frac{\Phi_1 + \Phi_2}{2}\right) 2\cos\left(\frac{\Phi_1 - \Phi_2}{2}\right) \tag{21}$$

2.2.2 CARM and DARM in the Idealized Case

Michelson interferometers measure differential arm length by splitting light into two perpendicular beams, sending them along a set of arms, then recombining them. If the beams have travelled different lengths (modulo the light's wavelength) then they will pick up a relative phase, and hence destructively interfere with each other when recombined. For an idealized interferometer with a monochromatic laser and perfect 50:50 beam splitter (see Figure 6), we can write the field at the detection photodiode (the anti-symmetric port) as:

$$E_S = E_0 \frac{i}{2}\Big(\exp(i2kL_Y) + \exp(i2kL_X)\Big) \tag{22}$$

Defining common and differential arm lengths as

$$\bar{L} = \frac{L_Y + L_X}{2} \tag{23}$$

and

$$\Delta L = L_Y - L_X \tag{24}$$

respectively, and noting that

$$\Phi_i = 2kL_i \tag{25}$$

we can reduce the above to

$$E_S = E_0 i \exp(i2k\bar{L})\cos(k\Delta L) \tag{26}$$

so that the intensity of the signal will be

$$P_0 \cos^2(2\pi\Delta L/\lambda) \tag{27}$$

When this is nearly 0 then the interferometer is on a *dark fringe*, and when it is nearly P_0 the interferometer is on a *light fringe*. Modern interferometers are operated at or near the dark fringe, for reasons which we will go into shortly.

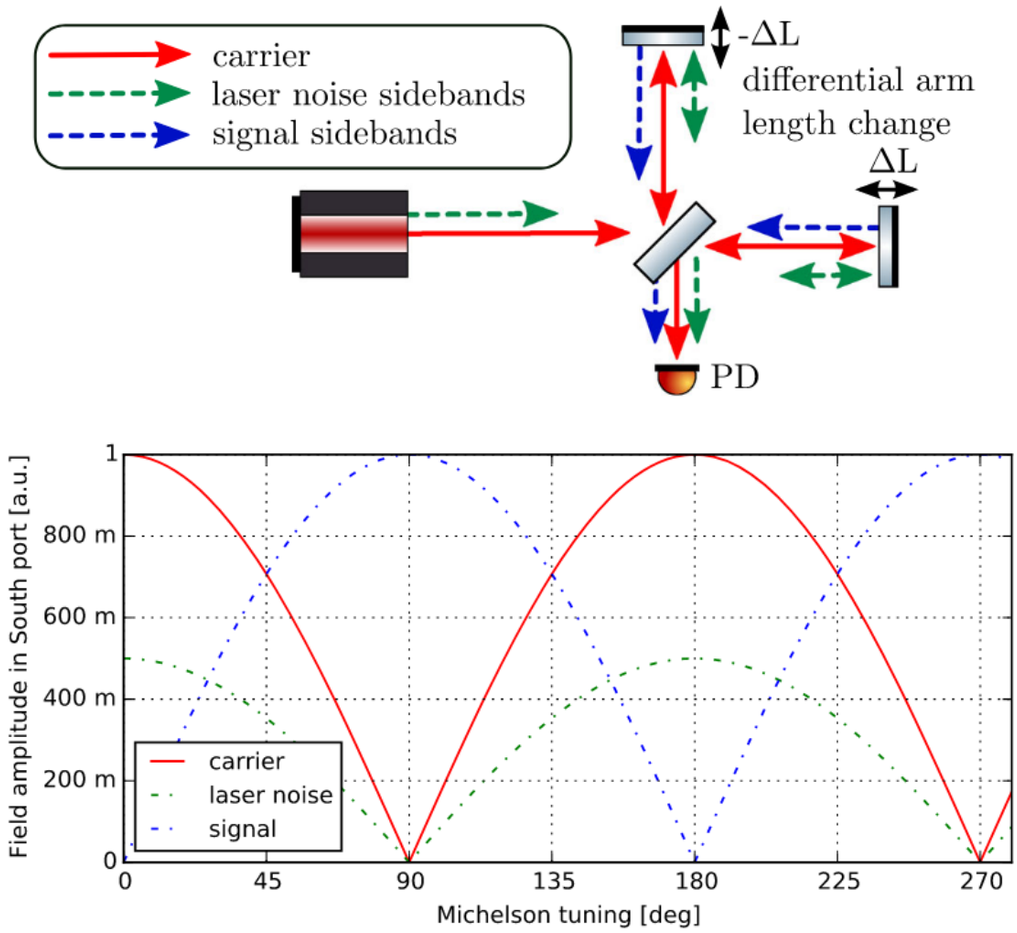

Figure 7: A schematic of sidebands in a Michelson inteferometer, and the effect of tuning on the carrier and the sidebands

3 Gravitational Wave Signal Detection

3.1 Modulation and Sidebands

3.1.1 Phase Modulation

Now, the next order of business is a digression about phase modulation. A phase modulated signal when a carrier field $E_{in} = E_0 \exp(i\omega_0 t)$ is modulated to

$$E = E_0 \exp\Big(i(\omega_0 t + m\cos(\Omega t))\Big) \tag{28}$$

To handle this mathematically we can invoke Bessel functions of the first kind (you remember those, surely?) by the identity:

$$\exp(iz\cos(\phi)) = \sum_{k=-\infty}^{\infty} i^k J_k(z)\exp(ik\phi) \tag{29}$$

For small modulation indices we can approximate the bessel functions by:

$$J_k(m) = \left(\frac{m}{2}\right)\sum_{n=0}^{\infty}\frac{-m^{2n}}{4^n n!(k+n)!} \approx \frac{1}{k!}\left(\frac{m}{2}\right)^k \tag{30}$$

Making use of the identity $J_{-k}(m) = (-1)^k J_k(m)$, we can get a second order expression for the phase modulated field:

$$E \approx E_0\exp(i\omega_0 t)\left[1 - \frac{m^2}{4} + i\frac{m}{2}\Big(\exp(-i\Omega t) + \exp(i\Omega t)\Big)\right] \tag{31}$$

Notably, this field now has *sidebands* at $\pm\Omega$.

3.1.2 Sidebands and Michelson Interferometer Tuning

Now, to consider how sidebands work in Michelson interferometers, take note of Figure 7. Per the equation derived above, we see that at $\pi/2$ and $3\pi/2$ tunings, the carrier power is minimized. So too is the laser noise, which is a common sideband source across all legs. What is interesting is that the signal sidebands are *maximized*; to understand why this is, recall our phase convention. Transmission through a mirror introduces a phase of $\pi/2$, which reflection does not. The carrier and laser noise side bands will get a phase shift when entering the X arm, and when leaving the Y arm, such that they end up in the same phase. By contrast, the

signal sideband will *only* experience a phase shift in the Y arm, so if no tuning is applied it will be perfectly out of phase and destructively interfere, whereas if there is a $\pi/2$ phase applied it will suddenly be perfectly in phase and constructively interfere.

3.1.3 The Homodyne Detection Scheme

Figure 7 shows that noise is minimized and signal maximized at the dark fringe, but there is a bit of a catch. The absolute magnitude of the signal sidebands is very small, and so to improve detectability we need something to beat against. There are a number of solutions to this problem, but the one used by LIGO is called a *homodyne* scheme. Essentially, the interferometer is held very slightly off of the dark fringe - how that is done has to do with the control systems, so let's just say we can do it and leave it at that for now. So

$$\Delta L = \frac{\pi}{2k_0} + \delta_{off} \tag{32}$$

for $k_0 = \omega_0/c$ (the wavenumber of the carrier field). The DC offset δ_{off} is held at a very small but non-zero value. Using equations 21 and 31 we can write this as

$$\begin{aligned} E &= irtE_0 \exp(i2k_0\bar{L}) \exp(i\omega_0 t)(2\cos(k_0\Delta L) + s^+ + s^-) \\ &= irtE_0 \exp(i2k_0\bar{L}) \exp(i\omega_0 t)(2\sin(k_0\delta_{off}) + s^+ + s^-) \end{aligned} \tag{33}$$

from which we can get the transmitted power:

$$P = EE^* = TR|E_0|^2\bigg(4\sin^2(k_0\delta_{off}) + 2\sin(k_0\delta_{off})(s^+ + s^-) + O(s^2)\bigg) \tag{34}$$

Hence we see the necessity of including a bit of the carrier signal.

3.2 Response to a GW

We can compute the phase due to an impending GW:

$$\phi = -k_0 L \mp \frac{\omega_0}{2}\int_{t-L/c}^{t} h(t) = -k_0 L \mp \delta\phi \tag{35}$$

Considering a very simple gravitational wave:

$$h(t) = h_0 \cos(\omega_{gw} t + \phi_{gw}) \tag{36}$$

We can compute

$$\delta\phi = \frac{\omega_0 h_0}{\omega_{gw}} \cos\bigg(\omega_{gw} + \phi_{gw} - \frac{\omega_{gw} L}{2c}\bigg) \sin\bigg(\frac{\omega_{gw} L}{2c}\bigg) \tag{37}$$

Going back to our phase modulation equation 28 we can identify

$$m_{gw} = -\frac{\omega_0 h_0}{\omega_{gw}} \sin\bigg(\frac{k_{gw} L}{c}\bigg) \tag{38}$$

and

$$\Phi = -\frac{k_{gw} L}{2} + \phi_{gw} \tag{39}$$

where $k_{gw} = \omega_{gw}/c$. So we can proceed and work out

$$A_{gw} = \frac{m_{gw}}{2} = -\frac{\omega_0 h_0}{2\omega_{gw}} \sin\bigg(\frac{k_{gw} L}{c}\bigg) \tag{40}$$

$$\Phi^{\pm}_{gw} = \frac{\pi}{2} - Lk_0 \pm \bigg(-\frac{k_{gw} L}{2} + \phi_{gw}\bigg) \tag{41}$$

$$\alpha^{\pm}_{gw} = A_{gw} \exp(i\Phi^{\pm}_{gw}) \exp(\pm i\omega_{gw} t) \tag{42}$$

Now looking to the schematic in Figure 8, we can write out the expressions for each optical propagation element:

$$a_3 = a_2 \exp(-ik_0 L) \tag{43}$$

$$a_2 = r_{etm} a_1 \tag{44}$$

$$a_1 = a_0 \exp(-ik_0 L) \tag{45}$$

and

$$b^{\pm}_1 = a_0 \alpha^{\pm}_{gw} \tag{46}$$

$$b^{\pm}_2 = r_{etm} b^{\pm}_1 \tag{47}$$

$$\begin{aligned} b^{\pm}_3 &= b^{\pm}_2 \exp(-i(k_0 \pm k_g w)L) + a_2 \alpha^{\pm}_{gw} \\ &= 2r_{etm} a_0 \alpha^{\pm}_{gw} \exp\bigg(-ik_0 L \mp i\frac{k_{gw} L}{2}\bigg) \cos\bigg(\mp i\frac{k_{gw} L}{2}\bigg) \\ &= -i\frac{r_{etm} a_0 \omega_0 h_0}{2\omega_{gw}} \sin(k_{gw} L) \exp(-i2k_0 L) \exp(\pm i(\omega_{gw} t - k_{gw} L + \phi_{gw})) \end{aligned} \tag{48}$$

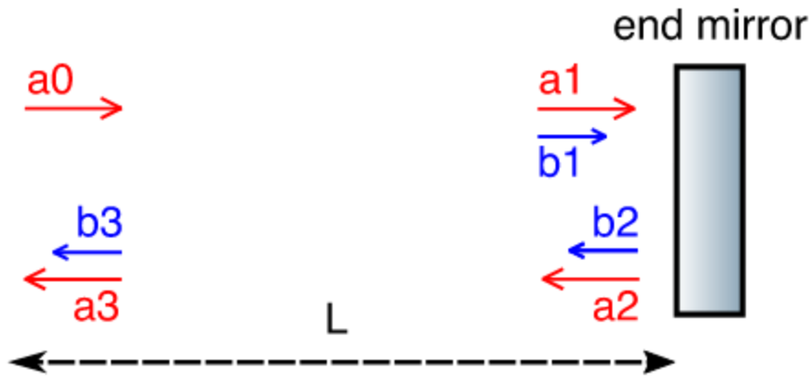

Figure 8: A schematic of the propagation of the carrier beam and the signal sidebands in one interferometer arm

Now, for each arm respectively

$$b_X^{\pm} = b_3^{\pm}(L = L_X, a_0 = itE_0) \tag{49}$$

and

$$b_Y^{\pm} = b_3^{\pm}(L = L_Y, a_0 = rE_0) \tag{50}$$

So that

$$E_{out} = i2rtE_0\cos(k_0\Delta L) + b_X^+ + b_X^- + b_Y^+ + b_Y^- \tag{51}$$

After recombining in the output port, these go to

$$b_Y^3 = \frac{rtE_0\omega_0 h_0}{2\omega_{gw}}\sin(k_{gw}L_Y)\exp(-i2k_0L_Y)\exp(\pm i(\omega_{gw}t - k_{gw}L_Y + \phi_{gw})) \tag{52}$$

$$b_X^3 = -\frac{rtE_0\omega_0 h_0}{2\omega_{gw}}\sin(k_{gw}L_X)\exp(-i2k_0L_X)\exp(\pm i(\omega_{gw}t - k_{gw}L_X + \phi_{gw})) \tag{53}$$

The negative sign on the X arm is our kludgy implementation of the antenna response to this polarization. Now, we can switch this to CARM and DARM, and assume a perfect 50:50 splitter. Furthermore, LIGO detectors are set to $k_{GW} >> \Delta L$, such that $k_{gw}(\bar{L} + \Delta L/2) \approx k_{gw}\bar{L}$. So, taking all this and summing, we get the field (also using the fact that for our homodyne scheme $\sin(2k_0\Delta L) \approx 2k_0\delta_{off}$

$$E_{out} = iE_0\cos(k_0\Delta L) - i\frac{2k_0\delta_{off}E_0\omega_0 h_0}{\omega_{gw}}\sin(k_{gw}\bar{L})\cos(\omega_{gw}t - k_{gw}\bar{L} + \phi_{gw}) \tag{54}$$

and power due to the gravitational wave is

$$P_{gw} \approx 2k_0\delta_{off}\frac{\omega_0 h_0}{\omega_{gw}}|E_0|^2\sin(k_{gw}L)\cos(\omega_{gw}t - k_{gw}\bar{L} + \phi_{gw}) \tag{55}$$

This also gives the transfer function

$$T_{gw\to P}(\omega_{gw}) \approx k_0\delta_{off}|E_0|^2\frac{\omega_0}{\omega_{gw}}\sin(k_{gw}\bar{L})\exp(-ik_{gw}\bar{L}) \tag{56}$$

4 Noise Sources

4.1 Shot Noise

Shot noise is a fundamental source of noise due to vacuum fluctuations - it can never be removed, but increasing the circulating power in the detector allows us to mitigate it. The noise PSD due to shot noise is given by:

$$S_{P,DC} \approx 2P_0(k_0\delta_{off})^2\hbar\omega_0 \tag{57}$$

Combined with the noise transfer function given in equation 56, we can get the noise signal ratio:

$$NSR = \frac{\sqrt{S_{P,DC}}}{T_{gw\to P}} = \sqrt{\frac{2\hbar}{P_0\omega_0}}\frac{\omega_{gw}}{\sin(\omega_g w\bar{L}/c)}\frac{h}{\sqrt{Hz}} \tag{58}$$

Importantly, this decreases with the square root of *carrier* power, and has a sharp feature at the free spectral range of the arm (though this doesn't come up very often in the LIGO detectors, since noise is already to high for detectability by then). Figure 9 shows what this looks like.

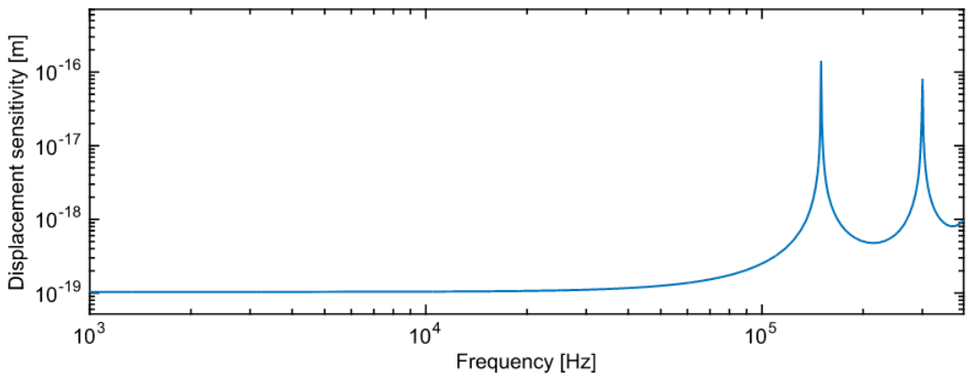

Figure 9: Shot noise sensitivity limit for $P_0 = 1\ W$ and $L = 1\ km$

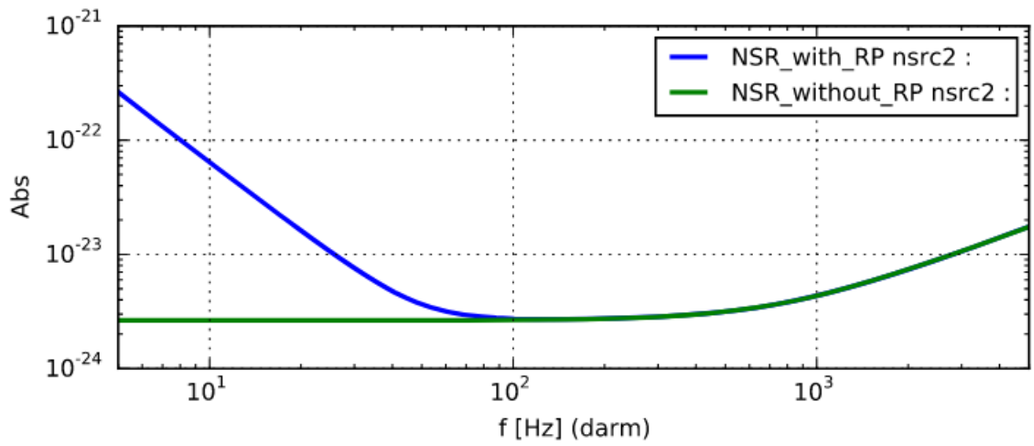

Figure 10: Sensitivity limits due to both shot noise and radiation pressure

4.2 Radiation Pressure

Radiation pressure is another fundamental noise source, which results in a power spectral density:

$$S_{\phi,RP} = \frac{8\hbar P_0^3 \omega_0 k_0^2}{M^2 c^2 \Omega^4} \tag{59}$$

So the NSR due to this will be

$$\sqrt{\frac{8\hbar P_0}{\omega_0}} \frac{1}{\delta_{off} M c \omega_{gw}^2 \sin(\omega_{gw} \bar{L}/c)} \tag{60}$$

Notably this *increases* with the square root of power, but it decreases with the square of the frequency, and so is principally a low frequency noise source. The combined effect of radiation pressure and shot noise can be seen in Figure 10. The full noise breakdown of the aLigo design (note, this is not the same as what actually exists) is seen in Figure 11

5 Modern Interferometer Design Elements

5.1 Power Recycling

As can be seen in the above discussion of shot noise, if we wish to decrease our noise floor it is necessary to increase our power. However, increasing the raw laser power past a certain point begins to sacrifice stability to an unacceptable degree, and so it is desirable to instead amplify the laser by optical methods. This is the purpose of the power recycling cavity, which essentially "catches" power leaking from the symmetric port and puts it back into the detector. This provides a gain in power proportional to the finesse of the PRC:

$$G_{PR} \approx \frac{\mathcal{F}}{\pi} \tag{61}$$

Figure 12 shows what this looks like schematically.

5.2 Arm Cavities

Adding Fabry-Pérot cavities to the arms of the detector also allows an increase in power, both in the carrier and, to an even greater extent, the signal sideband. Moreover, they increase the effective length of the arms, since photon lifetimes within the arms are significantly increased. Figure 13 shows the schematic of what this looks like.

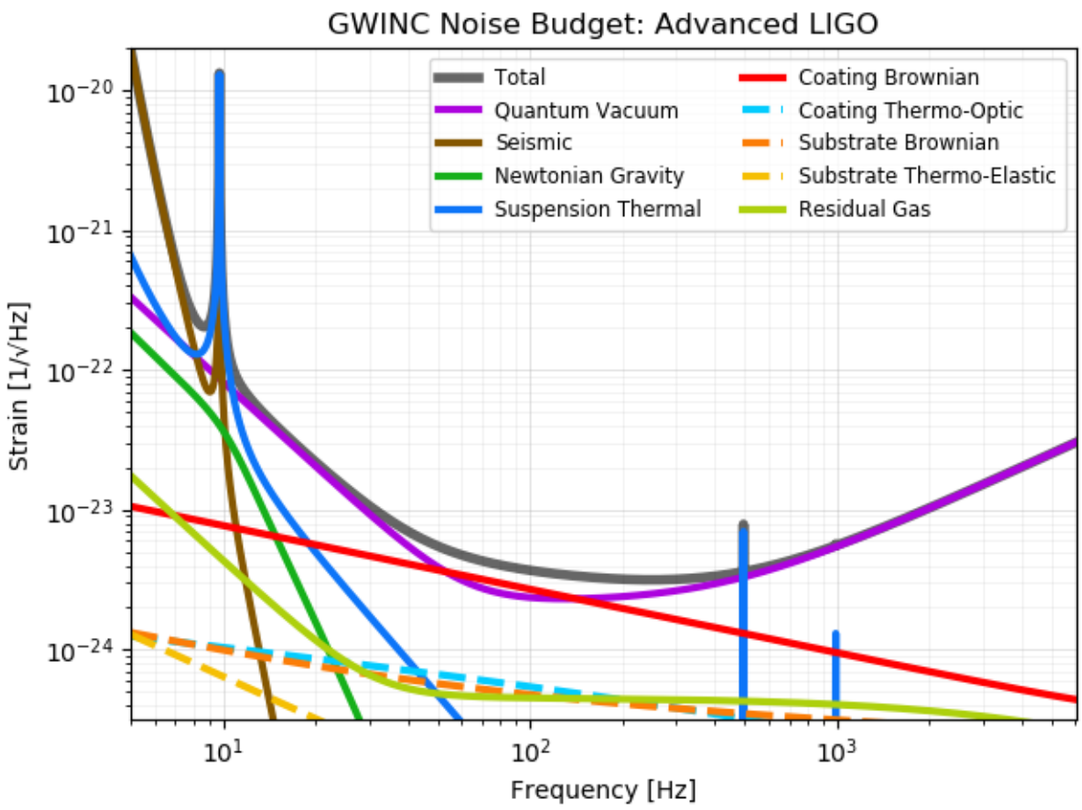

Figure 11: Breakdown of noise sources in aLigo according to the GWINC model[3]

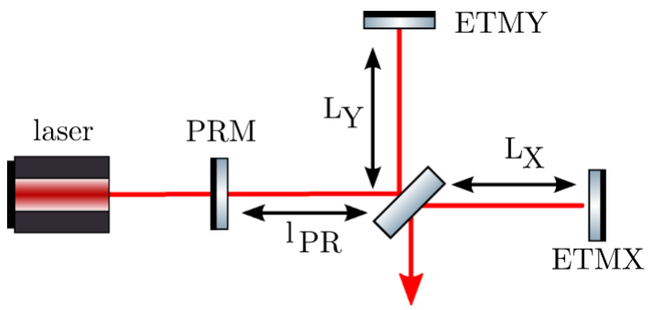

Figure 12: The layout of an interferometer with a power recycling cavity added

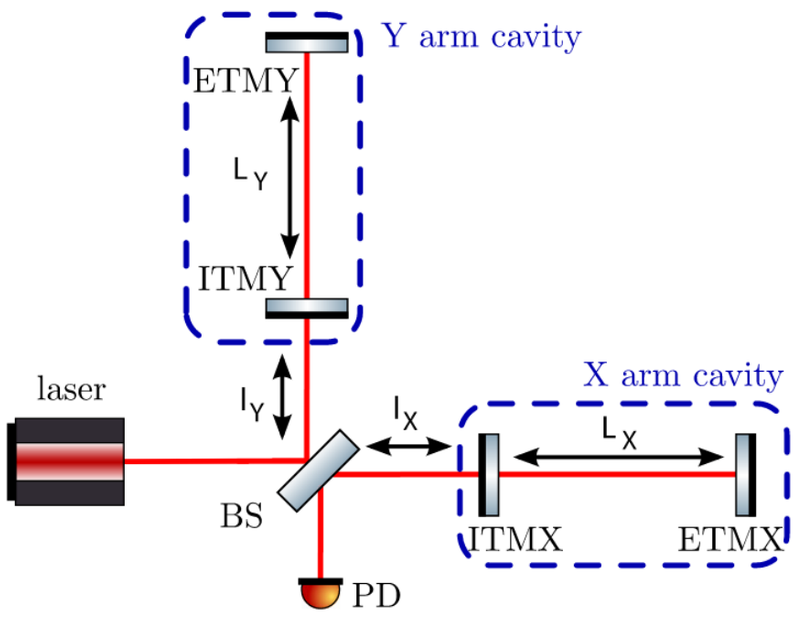

Figure 13: The layout of an interferometer with arm cavities added

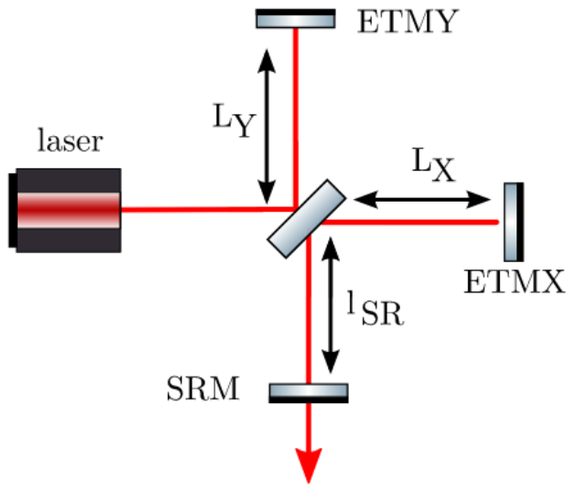

Figure 14: The layout of an interferometer with a signal recycling cavity added

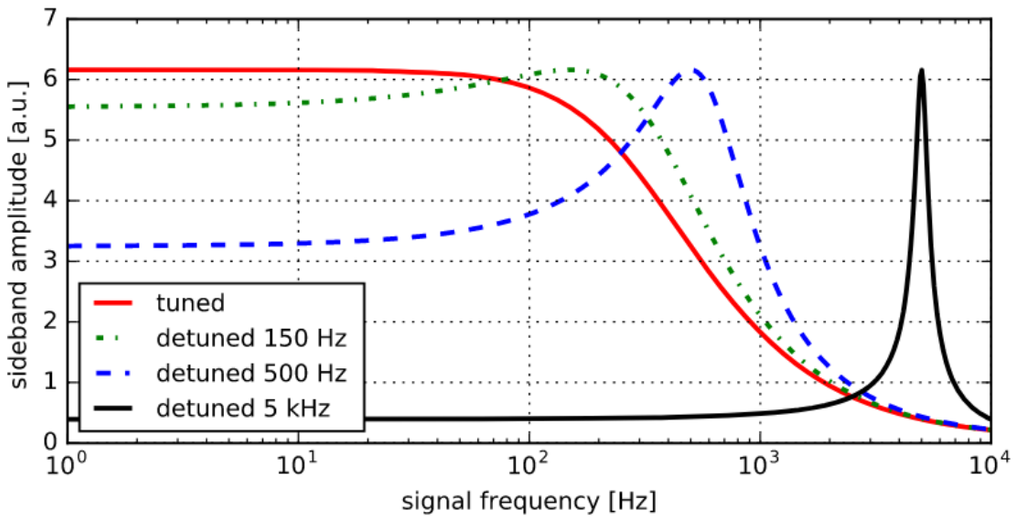

Figure 15: Sideband amplitude for various tunings of the SRC

5.3 Signal Recycling

A signal recycling cavity is a Fabry-Pérot cavity placed at the output port, which allows for resonant sideband extraction. If the finesse of arm cavities above is very high, then a very sharp resonant feature is developed, narrowing the bandwidth. The SRC is tuned to an *anti*-resonant operating point, which increases the bandwidth of the detector. The design of this may be seen in Figure 14. The effect of tuning on the sideband sensitivity can be seen in Figure 15.

References

[1] Charlotte Bond et al. "Interferometer techniques for gravitational-wave detection". In: *Living Reviews in Relativity* 19.1, 1 (Dec. 2016), p. 1. DOI: 10.1007/s41114-016-0002-8.

[2] Benjamin P. Abbott et al. "The basic physics of the binary black hole merger GW150914". In: *Annalen Phys.* 529.1-2 (2017), p. 1600209. DOI: 10.1002/andp.201600209. arXiv: 1608.01940 [gr-qc].

[3] Jameson Graef Rollins et al. *pygwinc: Gravitational Wave Interferometer Noise Calculator*. Astrophysics Source Code Library, record ascl:2007.020. July 2020. ascl: 2007.020.